

The Filler Effect: The Influence of Filler Content and Surface Area on Cementitious Reaction Rates

Tandré Oey (*), *Aditya Kumar* (†), *Jeffrey W. Bullard* (‡), *Narayanan Neithalath* (§), *Gaurav Sant* (**, ††)

Abstract

Finely ground mineral powders are known to accelerate cement hydration rates. This “filler effect” has been attributed to the effects of dilution (w/c increase) when the cement content is reduced or to the provision of additional surface area by fine powders. The latter contribution (i.e., surface area increase) is speculated to provide additional sites for the nucleation of the hydration products, which accelerates reactions. Through extensive experimentation and simulation this paper describes the influence of surface area and mineral type (e.g., quartz or limestone) on cement reaction rates. Simulations using a boundary nucleation and growth (BNG) model and a multiphase reaction ensemble (MRE) indicate that the extent of the acceleration is linked to the: (1) magnitude of surface area increase and (2a) capacity of the filler’s surface to offer favorable nucleation sites for hydration products. Other simulations using a kinetic cellular automaton model (HydratiCA) suggest that accelerations are linked to: (2b) the interfacial properties of the filler that alters (increases or decreases) its tendency to serve as a nucleant and (3) the chemical composition of the filler and the tendency for its dissociated ions to participate in exchange reactions with the calcium silicate hydrate product. The simulations are correlated with accelerations

* Research Assistant, Laboratory for the Chemistry of Construction Materials (LC²), Department of Civil and Environmental Engineering, University of California, Los Angeles, California, Email: tandre.oey@gmail.com

† Scientist, Laboratory for the Chemistry of Construction Materials (LC²), Department of Civil and Environmental Engineering, University of California, Los Angeles, California, Email: adityaku@ucla.edu

‡ Materials Engineer, Engineering Laboratory, Materials and Construction Research Division, National Institute of Standards and Technology, Gaithersburg, Maryland, Email: bullard@nist.gov

§ Associate Professor, School of Sustainability and the Built Environment, Arizona State University, Tempe, Arizona, Email: narayanan.neithalath@asu.edu

** Assistant Professor and Rice Endowed Chair in Materials Science (Corresponding Author), Laboratory for the Chemistry of Construction Materials (LC²), Department of Civil and Environmental Engineering, University of California, Los Angeles, California, Email: gsant@ucla.edu

†† Member, California Nanosystems Institute, University of California, Los Angeles, California

observed using isothermal calorimetry when fillers partially replace cement. The research correlates and unifies the fundamental parameters that drive the filler effect and provides a mechanistic understanding of the influence of filler agents on cementitious reaction rates.

Keywords: cement hydration, filler, limestone, quartz, boundary nucleation and growth, surface area

1.0. Introduction and Background

Environmental considerations are creating an increasing demand to reduce the use of portland cement in concrete mixtures [1,2]. Reductions in cement use are often achieved by dilution, i.e., by replacing a portion of the cement with filler materials such as limestone or fly ash, which may be inert or reactive during the course of hydration. Unfortunately, the dilution of cement can adversely impact the rate or extent of development of properties such as strength [3,4,5]. The negative consequence on properties often impedes the practical acceptance of formulations with high volumes of cement replacement due to issues of reduced or retarded constructability when using these materials [6,7].

Dilution, however, is not the only possible effect of fillers. Some mineral replacements, such as fine limestone, have been correlated with accelerated cement hydration rates at early ages [8,9,10,11]. This acceleration has been attributed to two main phenomena: (1) enhanced heterogeneous nucleation of hydration products due to the increased surface area provided by fine filler powders, and (2) greater amount of water per unit mass of cement particles (i.e., w/c increase or dilution) [8,12,13,14,15,16,17]. Such accelerations may be beneficial, especially at early ages, when an increase in the degree of cement hydration may be able to partially offset the detrimental effects of reduced cement content on hardened properties. Therefore, a more comprehensive understanding of the influences of different fillers could enable new strategies for optimizing sustainable mixture designs, by which particular fillers could be

intelligently chosen for their ability to “dial in” a desired rate and extent of hydration and property development in cementing systems [18].

Several studies have already demonstrated “mineral accelerations”, but the majority of studies have emphasized aspects of property development and mixture proportioning, when the cement content is reduced [19]. Systematic investigations describing the influences of available surface area and dilution on hydration reactions are much rarer. Of these, most studies have evaluated individual mineral powders (e.g., quartz, rutile, anatase, limestone, silica fume, synthetic C-S-H [9,10,11,20,21,22,23]) in detail, instead of comparing the relative capacities of different fillers to accelerate hydration. In contrast, the present study uses both experiments and a combination of simulation methods to deconvolute the effects of the filler content (i.e., cement replacement level and w/c increase) and surface area (i.e., fineness) on hydration rates. Computer simulations are applied to describe how a change in the nature and area of the solid surfaces influences reactions [24,25,26]. Special efforts are made to describe the mechanism of reaction acceleration for two filler agents, i.e., limestone and quartz at early ages. The outcomes provide a means for concrete technologists to develop cementitious binders and concretes with reduced clinker factors (for cement) and reduced cement contents (for concretes), which could display similar properties as traditional portland cement systems.

2.0. Materials and Experimental Methods

An ASTM C150 compliant Type I/II ordinary portland cement (OPC) with an estimated Bogue phase composition of 59% C_3S , 16% C_2S , 4% C_3A , 11% C_4AF and a Na_2O equivalent of 0.40% was used in this study. The limestone and quartz powders used are commercially available (nominally pure) particle size classified products produced by OMYA A.G. and the U.S. Silica Company. The particle size distributions (PSD, Figure 1) of all the solids were measured using a Beckman Coulter Light Scattering Analyzer (LS13-320) using isopropanol and sonication for dispersing the powders to primary particles. The

uncertainty in the light scattering analysis was determined to be approximately 6% based on multiple measurements performed on six replicate samples assuming the density of the cement, limestone and quartz to be 3150 kg/m³, 2700 kg/m³ and 2650 kg/m³ respectively.

Figure 1: Particle size distributions for the: (a) cement, (b) limestone and (c) quartz used in this study. The uncertainty in the measured particle size distribution is around 6 %.

Cementitious paste mixtures were prepared using de-ionized (DI) water at a fixed water-to-solids ratio ($w/s = 0.45$) using a planetary mixer as described in ASTM C305 [27]. To better understand the role of filler agents, the cement content was progressively reduced (by replacement) in 10% increments from 0-50% (mass-basis) by limestone and quartz powders of varying particle sizes (Figure 1 and Table 1).

The influence of powder additions (i.e., cement replacement) on the solid surface area of the system is shown in Figure 2 and is described using an area multiplier (AM, unitless) as shown in Eq. (1):

$AM = 1 + \frac{r \text{ SSA}_{filler}}{(100 - r) \text{ SSA}_{cement}}$	(1)
--	-----

where r (mass %) is the percentage replacement of cement by filler (limestone or quartz) and SSA_{cement} and SSA_{filler} (m²/g) are the specific surface areas of the cement and filler, respectively, calculated from the particle size distribution and the particle density, while assuming spherical particles. It should be noted, given the irregular, angular nature of the particles considered, the spherical particle assumption, likely results in imprecisions in determinations of the surface area. Thus, AM is a scaling factor that describes the (relative) change in solid surface area induced by filler addition in comparison to the surface area provided by a unit mass (1 g) of cement. In other words, AM is the surface area of filler per unit surface area of cement in the system. The greater this quantity is, either because the filler is finer or because it is

present in greater amounts, the more AM will exceed unity. It should be noted that the calculation of the AM is subject to uncertainties that stem from measurements of the particle size distributions.

Figure 2: The correlation between the level (mass) of cement replacement and the change induced in the available solid surface area in the system for: (a) limestone and (b) quartz powders. The uncertainty in the calculated AM stems from the uncertainty inherent to the particle size analysis and is correspondingly around 6 %.

Table 1: Nominal d_{50} and specific surface area (SSA) values, as calculated using the measured particle size distribution (Figure 1), for the cement, quartz and limestone used in this study. The uncertainty in the measured d_{50} and SSA are both around 6 %.								
	Cement		Limestone			Quartz		
ID	Size (d_{50}) (μm)	SSA (m^2/kg)	ID	Size (d_{50}) (μm)	SSA (m^2/kg)	ID	Size (d_{50}) (μm)	SSA (m^2/kg)
Cement	10.78	486.60	0.7	1.40	2592.10	10.0	3.81	1610.00
			3.0	2.98	1353.20	40.0	7.42	464.50
			15.0	14.87	399.20	75.0	17.24	270.20
			40.0	40.10	228.60	20-30 Sand	783.00	2.80

The influence of cement replacement on the rate of reactions was tracked using isothermal conduction calorimetry. A TamAir isothermal calorimeter (TA Instruments^{††}, DE, USA) was used to determine the heat evolved during hydration, of externally mixed pastes, at a constant temperature condition of 25°C. The thermal power and energy measured were then used to assess the influence of powder additions on reaction kinetics and cumulative heat release of the cementitious pastes. The uncertainty in the measured

^{††} Certain commercial materials and equipment are identified to adequately specify experimental procedures. In no case does such identification imply recommendation or endorsement by the University of California, Los Angeles, the National Institute of Standards and Technology, or Arizona State University, nor does it imply that the items identified are necessarily the best available for the purpose.

heat flow rate was determined to be around ± 2 % based on the heat flow measured on six replicate specimens between 1 hour and 72 hours.

3.0. Experimental Results: Assessing the Heat Release Response using Isothermal Calorimetry

Figure (3) shows representative heat evolution profiles for plain and binary (i.e., cement and limestone or cement and quartz) pastes for different levels of cement replacement. As denoted by the left-shift of the rate curve, the rate of reactions increases with the cement replacement level and filler fineness. It is noted that even for equivalent contributions of solid surface area, limestone is a better accelerant of hydration reactions than quartz (Figure 4).

Figure 3: Measured heat evolution profiles for binary paste systems prepared for $w/s = 0.45$. For a given mixture, the uncertainty in the measured heat flow is around 2 % based on the heat flow measured on six replicate paste specimens between 1 hour and 72 hours.

Given the large quantity of data produced, to describe the heat release responses of the mixtures, and their differences with respect to the (pure cement paste) reference more quantitatively, the heat curves were parameterized to determine the: (a) slope during the acceleration regime, (b) inverse of time elapsed from initial water contact to the main heat peak and (c) amplitude of the heat peak (i.e., the heat flow at the peak) for each mixture. Figure (5) indicates that the rates of reactions are enhanced in proportion with AM; both the slope during acceleration (Figure 5a) and the maximum heat flow rate increase (Figure 5b). Obviously, this acceleration corresponds to a reduction in the time required to reach the peak (Figure 5c). Further, note that all points but one are within 10% bounds of the best fit trend lines; the lone exception, corresponding to a high AM value (0.7 μm limestone, 50% replacement), which shows less than expected acceleration. This deviation likely results from: (1) enhanced agglomeration of fine filler particles, which would effectively act to reduce their exposed surface area and would trap water in flocs inducing a less than expected acceleration in hydration rates and/or (2) a surface area saturation effect, wherein for $AM > 4$, the available surface area is far more than is needed for reaction of the available quantity of cement,

resulting in a plateau in the measured reaction parameters. A parallel publication, details simple analytical methods by which reaction parameters, such as those illustrated in Figure 5 can be related to property (compressive strength) development in cementing materials. [28].

To compare their relative influences, it should be noted from Figure 5 that both limestone and quartz accelerate hydration reactions in terms of reducing the time to the heat peak and increasing the peak height at equal AMs. But the effect is much more pronounced for limestone than for quartz according to both of these measures, as also noted in Figure (4).

Figure 4: (a and b) Measured heat profiles for plain and binary pastes for equivalent AM values and (c) measured heat profiles for plain cement pastes prepared at different w/c . For a given mixture, the uncertainty in the measured heat flow is around 2 % based on the heat flow measured on six replicate paste specimens between 1 hour and 72 hours.

Figure 5: The correlation between the area multiplier (AM) and parameters corresponding to the measured heat flow profiles: (a) slope of the acceleration regime and (b) heat rate at the main peak (c) inverse of time to main peak. In all graphs, the solid line fits the linear portion of the dataset and the dashed line projects a linear extrapolation. The thin solid lines show a 10 % bound to the best-fit line. For a given mixture, the uncertainty in the measured heat flow is around 2 % based on the heat flow measured on six replicate paste specimens between 1 hour and 72 hours.

To further quantify the heat release response and deconvolute the effects of dilution and of increased surface area, a set of plain cement pastes were prepared with w/c ratios corresponding to the actual cement content in the systems with partial filler replacement levels ranging from 0 % to 30 % by mass (Figure 4c). In spite of a changing w/c , (since $AM = 1$ for all systems), the heat flow rates normalized by mass of cement are essentially identical. This result strongly suggests that the reaction kinetics are basically independent of water content unless additional surface area is provided by fillers. This result may suggest that, for the range of plain pastes and the w/c evaluated, the amount of water available to the reactant particles (i.e., the water to cement distance function) in realistic systems is broadly similar, and is

mainly a function of a similar level of solid agglomeration in these systems. Similar results have been noted for phase pure alite hydration at similar water contents [24,29,30,31,33], suggesting that this effect is likely not a function of the cement chemistry. Of course, there must be a lower limit of w/c (often applicable for $w/c < 0.42$) below which cement hydration rates begin to be influenced by the growing scarcity of water, especially at later ages as hydration progresses and self-desiccation occurs [32,33].

4.0. Computational Simulations of the Heat Release Response

To more rigorously interpret the calorimetric parameters, the heat release response was simulated using three models: (1) boundary nucleation and growth (BNG), (2) a multiphase reaction ensemble (MRE) and (3) kinetic cellular automaton model (HydratiCA). The simulations are applied to develop a mechanistic, physically consistent basis for understanding the influence of fillers on hydration reaction rates. It should be noted that the BNG and MRE models are only applied to simulate the post-induction period of hydration, and that their results presented here are the *best-fits* obtained for the corresponding (measured) systems. A best-fit is described as a simulation result that falls within a 5 % bound of the measured heat evolution profile for more than 90 % of the time between 2 h and 72 h. A sequence based on the simplex method is utilized to optimize the simulation parameters for a given system. The optimization procedure consists of: (a) providing w/c , SSA_{cement} and the measured heat flow as inputs, (b) defining different simulation variables as either *variable* or *fixed* (see summary below for fixed and variable parameters), and (c) defining constraints, or numerical bounds, on the variable simulation parameters. Initial guesses for fixed and variable parameters are the ones used for the paste system with no filler agent. The simplex method is invoked to iterate the values of the variable parameters within pre-defined constraints until the error between the measured and calculated rate curves is minimized between 2 h and 72 h. Through the iterations, the step size of each variable parameter is set at 0.0005 units and the numerical tolerance set to 10^{-14} . The optimization sequence is deemed to have converged when the magnitude of the difference in errors from two consecutive iterations is less than the set numerical tolerance; 10^{-14} . This convergence

criterion avoids the potential for numerical oscillations in the solution and yields the optimum values of the variable simulation parameters for a given system.

4.1. Classical Boundary Nucleation and Growth

Classical and modified forms of boundary nucleation and growth (BNG) models have been applied to describe the hydration of cementitious systems [24,34,35,36,37]. These models simulate reactions as a nucleation and growth process that starts at solid phase boundaries. In these models, a single product of a constant density is assumed to form, and its nucleation or growth is treated as the rate-controlling mechanism that determines the kinetics of the reaction [38]. BNG models have been formulated with a variety of assumptions for reaction mechanisms, including nucleation site saturation, product growth control, and the continued nucleation of product phases [24,26,38]. This study applies a modified form of a BNG formulation as shown in Eqs. (2-6) [39,40]:

$X = 1 - \exp \left[-2a_{BV} \int_0^{G_{out}t} (1 - \exp(-A_f)) dy \right]$	(2)
--	-----

where X is the volume fraction of the reactant transformed to product, G_{out} is the outward growth rate of the product, a_{BV} is the boundary area per unit volume, y is an integration variable, t is the simulation time (h), and A_f is the extended area (dimensionless) of the transformed product described in Eq. (3) and (4).

$A_f = \pi \left[I_{density} \cdot G_{par}^2 \cdot \left(t_r^2 - \frac{y^2}{G_{out}^2} \right) + I_{rate} \cdot G_{par}^2 \cdot \left(\frac{t_r^3}{3} - \frac{y^2 t_r}{G_{out}^2} + \frac{2y^3}{3G_{out}^3} \right) \right] \text{ if } (t_r > \frac{y}{G_{out}})$	(3)
<p style="text-align: center;">or</p> $A_f = \pi \left[N_{density} \cdot \left(t_r^2 - \frac{y^2}{G_{out}^2} \right) + N_{rate} \cdot \left(\frac{t_r^3}{3} - \frac{y^2 t_r}{G_{out}^2} + \frac{2y^3}{3G_{out}^3} \right) \right] \text{ if } (t_r > \frac{y}{G_{out}})$	
$A_f = 0 \text{ if } (t_r \leq \frac{y}{G_{out}})$	(4a)
$\text{where, } (t_r = (t - t_0))$	(4b)

where I_{density} (μm^{-2}) is the nucleation density of the product, that is, the starting number of supercritical nuclei per unit surface area, I_{rate} ($\mu\text{m}^{-2} \cdot \text{h}^{-1}$) is the nucleation rate, G_{par} ($\mu\text{m} \cdot \text{h}^{-1}$) is the growth rate parallel to the boundary surface, and G_{out} ($\mu\text{m} \cdot \text{h}^{-1}$) is the outward growth rate, perpendicular to the particle surface. Eq. (3) can also be expressed using N_{rate} (h^{-3}) and N_{density} (h^{-2}), which are respectively the products of the nucleation rate and nucleation density with the square of the parallel growth rate ($I_{\text{rate}} \cdot G_{\text{par}}^2$ and $I_{\text{density}} \cdot G_{\text{par}}^2$). The latter form, where the nucleation rate and nucleation density are convoluted with the parallel growth rate, is a more accurate representation of systems with anisotropic growth of product, because in these systems the fraction of area covered at a given distance from the nucleation (and growth) boundary depends on contributions from existing nuclei (present at a given time) and their growth rate along the boundary. Therefore, for a given N_{density} or N_{rate} , different combinations of I_{density} , I_{rate} and G_{par} may be permissible. The rate of heat release due to the hydration of the reactant (i.e., alite or cement) is computed using a scaling parameter, A (kJ/mol), as shown in Eq. (5):

$\frac{dH}{dt} = A \cdot \left(\frac{100}{100 - r} \right) \frac{dX}{dt}$	(5)
--	-----

where r (%) is the (mass) percentage replacement level of filler which accounts for the effects of dilution (i.e., a reduction in reactive cement content). In addition, the simulations begin only at the end of the induction period, so the simulation time is mapped to real time by using a parameter t_0 to designate the time at which the induction period ends as described by Eq. (4b). The boundary area per unit volume, a_{BV} (μm^{-1}), is calculated by adding the surface areas of the cement and filler and dividing by the system volume (total solids plus water):

$a_{BV} = \frac{SSA_{\text{cement}} \alpha_{\text{factor}} \rho_{\text{cement}} (100 f_{\text{cement}})}{V_{\text{free}}}$	(6)
--	-----

where f_{cement} (unitless) is the initial volume fraction of cement, ρ_{cement} is the density of the cement (3.15 g.cm^{-3}), V_{free} (μm^3) is initial volume of water present in the system and $\text{SSA}_{\text{cement}}$ is the specific surface area of cement fixed at $486.00 \text{ m}^2/\text{kg}$. The parameter a_{factor} (unitless) acts as a free variable representing a “virtual AM” used in the simulations. Based on the optimum parameters obtained for simulations of portland cement systems [43], for all simulations, the values of I_{rate} , G_{out} and G_{par} are fixed at $0.0 \mu\text{m}^{-2} \cdot \text{hour}^{-1}$, $0.03 \mu\text{m} \cdot \text{hour}^{-1}$ and $4.0 \mu\text{m} \cdot \text{hour}^{-1}$ respectively – indicative of a site saturation assumption. Next, f_{cement} (unitless) and a_{BV} (μm^{-1}) serve as input variables while A (kJ/mol), I_{density} (μm^{-2}), a_{factor} (unitless) and t_0 (hour) remain free (fitting) variables. Selection of a different value of G_{par} would lower or enhance the values of I_{density} proportionally, but would not otherwise alter the outcomes, or trends identified by the simulations. First, the best fit values of the simulation variables for the plain paste system were identified as rough estimates from prior work conducted on plain paste systems with similar surface areas and compositions and fine-tuned to properly describe the current paste system. Second, to fit the binary pastes with different levels of filler replacement, the simplex algorithm described earlier was applied to find the optimum parameters by varying: (1) I_{density} and a_{factor} from the values determined for the reference system to match the upslope and the time of peak through the acceleration regime, (2) the parameter A to be scaled so as to match the amplitude of the heat flow rate at the main peak, and (3) t_0 to shift the simulated heat flow response to the right (increase t_0) or to the left (decrease t_0) to temporally match the measured heat response.

Figure 6: Comparison of measured and BNG calculated heat profiles for paste mixtures. For a given mixture, the uncertainty in the measured heat flow is around 2% based on the heat flow measured on six replicate paste specimens between 1 hour and 72 hours.

Figure 6 shows representative best-fit simulation results for the reference and binary paste systems. Clearly, good fits are obtained for the reference system and for systems having low and intermediate levels of cement replacement. While the quality of the fit does slightly degrade at higher levels of cement replacement (approaching 50 %, mass basis), the BNG approach is broadly able to simulate the measured

heat response. The parameter optimizations suggest that A decreases with increasing replacement levels, although no systematic trend could be found in its variation with respect to filler content, type, or surface area [49]. The values of a_{factor} (i.e., virtual AM) are consistently less than the actual AM (Figure 7a) for both limestone and quartz systems. In fact, a_{factor} varies approximately linearly with AM, with slopes significantly less than unity. Nevertheless a_{factor} is much more sensitive to limestone replacement than to quartz replacement. This trend suggests that only a fraction of the filler's total surface area can offer preferential nucleation sites for the reaction products. However, a larger fraction or equal fraction at higher efficiency of the limestone surface participates in reactions compared to quartz. This aspect begins to explain how fine limestone is a more capable mineral acceleration agent than quartz, a point which is discussed in more detail below [41,42].

Next, the fitting parameters a_{factor} and $I_{density}$ are combined to calculate the number of supercritical product nuclei, N_{nuc} , produced per gram of reactant as shown in Eq. (7):

$N_{nuc} = (SSA_{cement} a_{factor}) I_{density}$	(7)
---	-----

Figure 7: (a) A comparison of the area factor (a_{factor}) plotted as a function of the area multiplier (AM) for systems simulated using the BNG mechanism and Product nuclei per gram of cement computed using the BNG approach as a function of: (b) replacement level for limestone systems (c) replacement level for quartz systems and (d) AM for limestone and quartz systems. Since the calculations are deterministic, for a given set of parameters the numerical solution shows no uncertainty.

The number of supercritical product nuclei produced per gram of cement is plotted against the level of cement replacement (Figures 7b and 7c) and AM (Figure 7d). Clearly, increasing cement replacement results in a proportional increase in the number of nuclei that participate in chemical reactions. This trend suggests increased product nucleation (i.e., higher $I_{density}$ values, while I_{rate} remains fixed) and therefore greater reaction rates in the presence of either mineral filler as compared to the plain cement system. However, limestone displays a substantially amplified nucleation response compared to quartz because,

both at equal replacement levels (Figure 7b and 7c) and equal AM values (Figure 7d), a larger number of product nuclei are initially generated in systems containing limestone. The divergence of the quartz and limestone response noted in Figure 7(d) correlates well with experiments (Figure 5). It is reasonable to expect that the number of nuclei would elevate with an increase in the surface area, but the important point here is that this response is filler specific. The divergence in the limestone and quartz responses is then indicative of the differing ability of these two mineral to serve as hydrate nucleation surfaces and mineral acceleration agents, with limestone showing a far greater surface affinity for the nucleation and growth of the cement hydrates – an observation that is supported by microscopy-based evidence provided by Sato and Diallo [42].

4.2. Multiphase Reaction Ensemble (MRE)

The Multiphase Reaction Ensemble (MRE) is a thermokinetic hydration model developed at EPFL [43]. It has been recently applied to simulate the progress of alite [44,45] and aluminate hydration [43], both as pure phases and as mechanical mixtures. The model uses inputs of the phase composition and particle size properties in conjunction with thermokinetic rules to simulate hydration [43,45]. Reasonably, the model considers no contributions from the belite and ferrite phases in the first 3 days of hydration [46]. First, to simulate alite hydration, the model applies a nucleation and densifying growth (NDG) criteria in which the C-S-H is assumed to grow with an increasing density with time [45,47]. More complete details of the model can be found elsewhere [43,45]. Briefly, the incremental amount of alite consumed by hydration in a time step dt is given by:

$-dm_{alite} = \frac{1}{k} \left[\left(\frac{\rho_{tr}}{\rho_0} (dV_{extended, CSH}(t + dt) - dV_{extended, CSH}(t)) (1 - V_{real, solid}) \right) + \left(\frac{\rho(t + dt) - \rho(t)}{\rho_0} V_{real, CSH} \right) \right]$	(8a)
<p style="text-align: center;">Here, $\frac{dV_{real, CSH}}{dt} = \frac{dV_{extended, CSH}}{dt} (1 - V_{real, solid})$</p>	(8b)

$V_{real,solid} = \frac{V_{solid,t} - V_{solid,t=0}}{V_{solid,t=0}}$	(8c)
--	------

The first term in Eq. 8(a) describes the amount of C-S-H formed and the second term describes the incremental change in volume of C-S-H that already exists (i.e., that was formed between time t_r and t), the parameter k is the ratio of the mass of alite reacted to the mass of C-S-H produced, t is the simulation time and ρ_0 (g. cm^{-3}) is the base density of C-S-H fixed at 2.10 g. cm^{-3} . $V_{real,C-S-H}$ (volume fraction) and $V_{extended,C-S-H}$ (volume fraction) are the volume fractions of the phase whose growth controls the kinetics, C-S-H in this case, without and with consideration of overlaps in surfaces, respectively, and $V_{real,solid}$ (volume fraction) is the fractional increase in the total volume of solids (V_{solid}) in the representative elementary volume ($REV = 100 \mu\text{m}^3$) at time t . These equations account for the space occupied by each phase (unreacted alite, portlandite and C-S-H) and the progressive change in the volume of C-S-H that is already present and continues to form with increasing hydration. The extended volume of the hydration product at any time can be calculated according to:

$V_{extended,CSH} = \int_0^{G_{out,t}} a_{BV}(1 - \exp(-A_f)) dy$	(9)
---	-----

The C-S-H density is assumed to vary exponentially in time according to:

$\rho(t) = \rho_{max} - (\rho_{max} - \rho_{min}) \cdot \exp\left[\frac{-k_{den} \cdot (t - t_0)}{(\rho_{max} - \rho_{min})}\right]$	(10)
--	------

where t_0 (h) is the start time parameter and ρ_{max} (2.10 g. cm^{-3}) is the final density of the outer C-S-H, ρ_{min} (g. cm^{-3}) is the initial density of outer C-S-H, k_{den} ($\text{g. cm}^{-3} \cdot \text{h}^{-1}$) is the rate of densification of outer C-S-H, a_{BV} is the boundary area of alite per unit volume (μm^{-1}) calculated using Eq. (6) with $SSA_{alite} = f_{alite} \cdot SSA_{cement}$. Here, f_{alite} is the mass fraction of alite in the cement determined using quantitative x-ray diffraction (QXRD). Based on prior experience, for these simulations, the values of I_{rate} , G_{out} , k_{den} and G_{par}

are fixed at $0.05 \mu\text{m}^{-2} \cdot \text{h}^{-1}$, $0.1035 \mu\text{m} \cdot \text{h}^{-1}$, $0.00055 \text{g} \cdot \text{cm}^{-3} \cdot \text{h}^{-1}$ and $1.0 \mu\text{m} \cdot \text{h}^{-1}$, respectively [43]. The free variables for the alite hydration sequence are ρ_{\min} ($\text{g} \cdot \text{cm}^{-3}$), I_{density} (μm^{-2}), a_{factor} (ratio) and t_0 (h).

Second, aluminate reactions were simulated in two stages [43]. Stage 1 describes C_3A hydration in a sulfated solution, which results in ettringite precipitation, and is modeled by a 1st order rate law:

$\frac{dm_{\text{C}_3\text{A}}}{dt} = -c_{\text{C}_3\text{A}} \cdot a_{\text{SA}} \text{ where,}$	(11)
$a_{\text{SA}}(t) = f_{\text{C}_3\text{A}} \cdot 4\pi((r_{\text{bulk}, t=0}) - k_1 t)^2 \text{ where,}$	(12)
$r_{\text{bulk}, t=0} = \left(\frac{3V_{\text{cement}}}{4\pi}\right)^{\frac{1}{3}}$	(13)

where V_{cement} (cm^3) is the volume of cement in the system, $f_{\text{C}_3\text{A}}$ is the C_3A content (mass fraction) of the cement, k_1 is a reaction rate constant ($\text{cm} \cdot \text{h}^{-1}$), t is the time (h) and $c_{\text{C}_3\text{A}}$ ($\text{g} \cdot \text{h}^{-1} \cdot \text{cm}^{-2}$) is a dimensional matching (normalization) constant. In this simplified model, therefore, the cement is assumed to be assembled into a single (hypothetical) spherical particle, the radius of which decreases with time, and the surface area of C_3A changes in proportion to that of the single particle. The values of k_1 and $c_{\text{C}_3\text{A}}$ were determined to be $0.125 \text{cm} \cdot \text{h}^{-1}$ and $7.59 \times 10^{-7} \text{g} \cdot \text{h}^{-1} \cdot \text{cm}^{-2}$ respectively [43].

Stage 2 of C_3A hydration covers the period after sulfate depletion, when ettringite does transform to monosulfate, and is modeled by a boundary nucleation and growth mechanism, Eqs. (2-5). This choice is based on observations of the hydration of model (mechanical) mixtures of C_3A -gypsum systems, in which the heat release, after gypsum depletion can be fit by a nucleation and growth equation [48,43]. For this stage, the values of G_{out} , G_{par} , I_{rate} , I_{density} and t_0 are fixed at $0.003 \mu\text{m} \cdot \text{h}^{-1}$, $1.0 \mu\text{m} \cdot \text{h}^{-1}$, $0.05 \mu\text{m}^{-2} \cdot \text{h}^{-1}$, $0.0 \mu\text{m}^{-2}$ and 18 h, respectively [43]. The value of a_{BV} is obtained using the value of a_{SA} from Eq. (12) at $t = t_0$, which represents the start time for monosulfate formation. The value of t_0 is fixed at 18 h for all systems considered, which corresponds to the time of gypsum depletion in the reference system, as determined from modeling of Stage 1.

Using the MRE model just described, alite hydration and aluminate hydration are assumed to be chemically decoupled, and therefore are treated separately so that the heat evolved from their respective reactions is added to obtain the heat profiles shown in Figure 8 [9]. Here too, based on prior simulation experience, the *best fit* values of the simulation variables for the plain system were first identified as estimates and then fine-tuned to properly describe the heat curve of the reference (plain paste) system. For binary paste systems, once again, the simplex algorithm described previously was used, with I_{density} and a_{factor} being varied from their values in the reference system to best match the upslope and the time of peak during the acceleration regime. In addition, ρ_{min} and t_0 were also varied to match the amplitude of the heat flow at the main peak (analogously to the parameter A) and to shift the simulated heat flow to the right (increase t_0) or left (decrease t_0) along the x-axis [49].

Figure 8: A representative set of simulated and measured heat evolution profiles for paste systems. The complete datasets from experiments and simulations are provided in the supplementary information. For a given mixture, the uncertainty in the measured heat flow is around 2% based on the heat flow measured on six replicate paste specimens between 1 hour and 72 hours.

Figure 8 shows representative best-fit simulation results for the reference and binary paste systems using the MRE model. Figure 8 shows that the MRE simulations are able to reliably replicate the experimental results for the entire range of systems and all cement replacement levels. However, major variations in a_{factor} (as relevant to the filler content and fineness) and I_{density} , and more limited variations in t_0 (-1.20 to -2.10 hours) and ρ_{min} (0.196-to-0.390 g.cm⁻³) were needed to obtain good fits [49]. It should be noted that variations in t_0 are applied to account for changes in the duration of the induction period (i.e., start time of the acceleration regime) because systems containing fillers often experience a slightly shorter induction period than the reference paste system. Although variations in ρ_{min} (increasing ρ_{min} with replacement level and filler fineness) are needed to scale the amplitude of the simulated heat flow, the specific nature of this variation or its correlation to a physical process is at this point fairly speculative [26,45].

Figure 9: Product nuclei per gram of cement computed using the MRE approach as a function of: (a) replacement level for limestone systems, (b) replacement level for quartz systems and (c) AM for limestone and quartz systems. Since the calculations are deterministic, for a given set of parameters the numerical solution shows no uncertainty.

As in the analysis of the BNG simulations, the nucleation density (I_{density}) and area factor (a_{factor}) are combined to calculate the number of supercritical product nuclei associated with a specific system. Figure 9 shows the number of nuclei as a function of the cement replacement level (Figure 9a and 9b) and as a function of AM (Figure 9c) for systems with limestone or quartz. Once again, increasing replacement of cement and solid surface area both increase the number of supercritical nuclei participating in the reactions. The divergence noted in the limestone and quartz systems (Figure 9c) is consistent with trends identified in the measured calorimetric parameters (Figure 5). Therefore, the MRE results, in agreement with the BNG simulations, imply that: (1) the additional surface area provided by fillers can enhance the nucleation of the hydration products and hence the rate and extent of early age hydration reactions, and (2) quartz and limestone can both enhance reaction rates, but limestone has a greater accelerating capacity than quartz at a given AM, due to its higher nucleation potential (i.e., number of supercritical nuclei produced and trends in I_{density}) – a conclusion supported by microscopy based evidence forwarded by Sato and Diallo [42].

4.3. Kinetic Cellular Automata Simulations (HydratiCA)

Cellular automata models have been used to simulate chemical and structural changes in space and time within systems by discretizing space and matter into uniform lattice sites and concentration quanta, respectively. A kinetic cellular automata model (HydratiCA) described for simulating diffusion, advection, and homogeneous standard rate kinetics in reactors [50] has been adapted in recent years to simulate chemical/structural evolution during early-age hydration of cement [51,52,53]. This model is applied to investigate how the thermodynamics and kinetics of C-S-H nucleation on surfaces of C_3S , limestone, and quartz can influence hydration and microstructure evolution at early ages. Chemical

changes and microstructural development are simulated by iterating over small time steps Δt , typically about 0.1 ms. Time steps are split into a transport step, during which mobile components in solution are able to move between lattice sites according to diffusion (random walk) or by perfect mixing (instant homogenization, as implemented in this study), and a reaction step, during which reactant species may combine to form products according to defined stoichiometric reaction equations^{§§}. The probability, p_i , of reaction i occurring at a lattice site depends on its relative rate constant, k_i , and on the number of cells $N_{a,i}$ of each reactant, a , involved in the reaction as shown in Eq. (14):

$p_i = k_i \xi^{\sum_a \nu_a} \Delta t \prod_a \max \left(0, \prod_{m=1}^{\nu_a} N_{a,i} - m + 1 \right)$	(14)
--	------

where: ξ is a constant model parameter that relates N_a to the molar concentration of component a , and ν_a is the molar stoichiometric coefficient of component a in the reaction. The relative rate constant is the product of the absolute forward rate constant, $k_{i,+}$, and the linearized thermodynamic driving force,

$k_i = k_{i,+} (1 - S_i)$	(15)
---------------------------	------

where: S_i , the saturation index for reaction i , is defined as the quotient $K_i / K_{i,eq}$ of its activity product and its equilibrium constant for the forward reaction. For heterogeneous reactions (i.e., reactions restricted to a surface) the surface area intersected by the lattice site must be multiplied on the right side. Eq. (15) is strictly valid only for elementary reactions (i.e., those involving one molecular step) but we have found it to be a useful approximation for many of the more complex dissolution and growth reactions that happen during cement hydration [51,52]. If k_i is negative in Eq. (15), the reaction is eligible to proceed in the

^{§§} Activities are estimated from molality's using activity coefficients calculated using the extended Debye-Hückel formula, which is a reasonable approximation when ionic strengths do not exceed a few tenths of mol/L.

reverse direction, in which case products are treated as reactants and vice versa for a given relative rate constant $|k_i|$. The reaction is allowed if p_i in Eq. (14) exceeds a random number drawn from a uniform distribution on $[0, 1]$. When a reaction happens, the number of cells of each reactant (product) at the affected lattice site is decremented (or incremented) by the number indicated by the molar stoichiometric coefficients ν .

Eqs. (14) and (15) are sufficient for modeling reaction kinetics involving dissolution, growth, sorption, and ion complexation. Since this study is concerned with the kinetics of hydration in the presence or absence of filler materials that might offer a reduced barrier for nucleation of C-S-H, to further consider these aspects, nucleation rates are modeled using classical nucleation theory [54]. The number of supercritical nuclei formed per unit volume per unit time (i.e., the nucleation rate) is given by Eq. (16):

$I = gS e^{-W^*/k_B T}$	(16)
-------------------------	------

where: g (s^{-1}) is the attempt frequency (or “frequency factor”), W^* (J) is the work required to form one supercritical nucleus, k_B is Boltzmann’s constant, and T is the absolute temperature (K). W^* itself is not a constant, but rather depends on temperature, the surface energy (γ , J/m^2), of the nucleating phase in the parent solution, and the saturation index, S , of the solution:

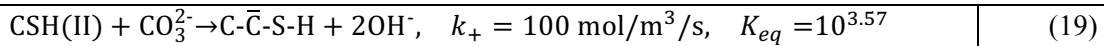
$W^* = \frac{A \Omega^2 \gamma^3}{k_B^2 T^2 \ln^2 S} = \frac{k_B w^*}{T^2 \ln^2 S}$	(17)
---	------

where A is a geometric factor, Ω is the molecular volume (m^{-3}) of the nucleating phase, and w^* (J) is approximately constant for a given nucleating material and parent solution. Thus, the rate Eq. (16) can be mapped to a probability equation similar to Eq. (14), except that in this case the relative rate constant k_i is replaced by k_{nuc} :

$k_{nuc} = k_0 \exp\left(\frac{-w^*}{T^3 \ln^2 S}\right)$	(18)
---	------

This stochastic model was used to simulate early hydration in a C₃S suspension (*w/s* = 0.45) with or without 10 % replacement by mass of quartz or limestone particles. The reactions and their associated thermodynamic and kinetic input parameters are either provided below, or are published elsewhere [52, 53, 59, 60, 61, 66]. Because simulations using this model are computationally intensive, and because our objective in using the model is simply to investigate the influence of C-S-H nucleation parameters on hydration rates, we simulate small systems containing a single C₃S particle, either 5 μm or 15 μm in diameter and, in selected simulations, a random dispersion of filler particles in the solution surrounding the C₃S particle. Periodic boundary conditions are invoked to compensate for the finite system volume.

In these simulations, the work of nucleation of either form of CSH on C₃S surfaces (*w**), is assumed to be 10^{10.83} K³, which is comparable to that for some inorganic salts nucleating in aqueous solutions. On limestone surfaces, the work of nucleation is assumed to be lower than this value by a factor of four. The attempt frequency is assumed to be 10^{14.2} s⁻¹. In systems with limestone replacement, we expect carbonate anions to be incorporated with C-S-H, to a limited extent, by analogy to the observed uptake of sulfate ions in systems containing gypsum [55]. Without reliable data for the reaction mechanism or its extent, we assume the same kind of ion exchange reaction as that used to model sulfate incorporation in CSH [56]:



As a first approximation, only the CSH(II) form is assumed to participate in the ion exchange reaction because the sorption tendency of anions should decrease with decreasing Ca/Si ratio as the zeta potential decreases [57]. In the case of limestone dissolution, we assume that the limestone used is pure calcite, with a dissociation reaction of: CaCO₃ → Ca²⁺ + CO₃²⁻. The forward rate constant is assumed to be k⁺ = 0.72 μmol/m²/s and the equilibrium constant is K_{eq} = 10^{-8.48}, with an enthalpy of reaction of -14.8 kJ/mol

(exothermic). A number of ion-ion complexation reactions can occur in solution, but only two are expected to occur to a significant degree:

$\text{CaOH}^+ \rightarrow \text{Ca}^{2+} + \text{OH}^-$, $k_+ = 0.06 \text{ mol/m}^3/\text{s}$, $K_{eq} = 0.0603$	(20)
$\text{CO}_3^{2-} + \text{H}_2\text{O} \rightarrow \text{HCO}_3^- + \text{OH}^-$, $k_+ = 0.06 \text{ mol/m}^3/\text{s}$, $K_{eq} = 10^{-3.67}$	(21)

The rate constants are chosen to be large enough that the reactions will happen very rapidly compared to other dissolution and growth reactions, but otherwise the values are arbitrary. The enthalpy of the former, carbonate reaction is 41 kJ/mol, i.e., endothermic. It is not possible to calculate the enthalpy of the other reaction from thermodynamic data, but it is not expected to make a significant contribution to the heat signature of a hydrating cementitious system.

Figure 10: (a) Simulations of heat released during the hydration of a single C_3S particle (5 μm or 15 μm) with no limestone filler (Reference), 10 % replacement of limestone filler (10% Limestone) with lower energy barrier of C-S-H nucleation and 10% replacement of quartz filler (10% Quartz) with energy barrier of C-S-H nucleation identical to C_3S and (b) Simulated influence on hydration rates of carbonate anion sorption on the C-S-H. All curves represent a single simulation; multiple simulations on similar systems indicate that the reproducibility of any curve is within 2 % at any point.

Figure (10a) shows the simulated cumulative heat release per gram of reactant for a system with either: a 5 μm C_3S particle or a 15 μm C_3S particle with no limestone filler, both of these systems each with 10 % mass replacement by limestone filler that offers a lower energy barrier than C_3S for C-S-H nucleation [42], and a system with the same replacement level for quartz filler where the energy barrier for the nucleation of C-S-H on quartz and on C_3S is equal. The latter consideration, i.e., of a similar nucleation potential of C-S-H on quartz as on C_3S has been recently confirmed by electron microscopy [58]. The model tracks heat release by multiplying the number of times each unit reaction occurs by the enthalpy change for each reaction. Enthalpies of the dissolution and precipitation reactions for phases including

C₃S, portlandite, C-S-H(I) and C-S-H(II), and for diffusive transport rates through the C-S-H forms are sourced from [52,53,59,60,61,66].

Figure (10a) shows that limestone causes a shortening of the induction period by as much as 50 % when it provides a lower C-S-H nucleation barrier (i.e., “a preferred filler effect”), although the effect is much greater for smaller particles. This behavior is also consistent with the BNG and MRE results already discussed. In contrast, no acceleration is predicted during the first 5 h of hydration when nucleation on a filler (in this case quartz) has the same energy barrier as on C₃S, although at later times the cumulative heat is slightly higher, perhaps due to more pronounced dilution (i.e., less C₃S initially implies a greater degree of reaction for the same amount of C₃S consumed). This behavior in the presence of a “non-preferred” filler is qualitatively similar to the heat response noted in presence of quartz fillers (Figure 3). However, in addition to these interfacial effects, limestone fillers can contribute carbonate anions to the pore solution, which can subsequently be incorporated within the C-S-H gel. This kind of uptake likely occurs through ion exchange reactions that release hydroxyl ions from the C-S-H to preserve charge neutrality. When limited carbonate incorporation is allowed by this kind of reaction (Eq. 19), the accelerating effect of the limestone is virtually unchanged at the beginning because it still offers the same preferential nucleation sites, as shown in Figure (10b). However, as more C-S-H is formed through hydration, progressively more ion exchange can occur. This is significant because OH⁻ ions released by the exchange reaction increase the driving force for C-S-H growth, by pH elevation [44,62], as compared to the driving force that evolves without CO₃²⁻ sorption. The result is an enhanced degree of reaction at later times. It should be mentioned that these conclusions are subject to refinement pending more accurate experimental characterization of the nature and limits of carbonate uptake in the C-S-H, studies of which are in progress at UCLA [63]. Nevertheless, in broad agreement with other studies, the simulations do indicate that a chemical effect driven by CO₃²⁻ ion sorption, in addition to a preferential nucleation effect, is responsible for enhanced hydration in cements containing limestone fillers. This ion sorption response

cannot be reproduced in the nominally inert quartz systems due to the inability of the silicate species to induce ion exchange reactions with the C-S-H^{***}.

5.0. Mechanistic Explanations of Accelerations in Cement Hydration Induced by Mineral Fillers

The outcomes of this study provide new insights into the influence of mineral fillers on accelerating the rate of reactions in cementitious materials. Simulations performed using nucleation and growth models and stochastic reaction-transport models indicate that the acceleration is produced by a combination of factors: (i) the filler fineness, (ii) interfacial properties and (iii) ion sorption/exchange effects. First, and perhaps not surprisingly, an increase in the filler fineness (i.e., solid surface area) accelerates hydration, but a balance is needed to ensure that concerns related to agglomeration, water trapping and surface area saturation do not detrimentally influence the system response.

The second important factor in determining filler effects is the collection of the interfacial properties of the cement and the filler material, which are critical for determining the extent and distribution of the nucleating hydration products. The energy barrier for heterogeneous nucleation on a surface is related to that for homogeneous nucleation of the same phase according to:

$\Delta G_{HET} = \Delta G_{HOM} \cdot \phi(\theta) = \left(\frac{16\pi\gamma_{PL}^3 V_M^2}{3\Delta\mu^2} \right) \cdot \left[\frac{(2 + \cos\theta)(1 - \cos\theta)^2}{4} \right]^n$	(18a)
$\cos\theta = \frac{\gamma_{SL} - \gamma_{PS}}{\gamma_{PL}}$	(18b)

where ΔG_{HET} is the energy that drives nucleation, applicable for the heterogeneous or homogenous case, $\Delta\mu = RT\ln(1+S)$ describes the supersaturation level with respect to the precipitating phase, R is the ideal

*** Amorphization of the quartz surface, during grinding, can result in a limited level of soluble silica in the system. However, this effect is negligible due to the low solubility of silica (far lower than CO₃²⁻ equilibrium), and as the amorphized layer, if present, resides in proximity to the particle surface and represents a negligible soluble volume.

gas constant, S is the saturation index of the precipitate in solution described previously, V_M is the molar volume of the precipitate, γ_{SL} is the substrate-liquid specific interface energy (J/m^2), γ_{PS} is the precipitate-substrate specific interface energy (J/m^2), γ_{PL} is the precipitate-liquid specific interface energy (J/m^2), θ is the thermodynamic contact angle, $\phi(\theta)$ is an activity factor (indicative of wetting, adhesion or surface affinity), which ranges between $[0,1]$, n is a constant ($n = 0.33$ for cap-shaped nuclei) and the subscripts P, L, and S indicate the precipitate (C-S-H), liquid, and solid substrate (i.e., limestone (l), quartz (q) or cement/C₃S (c)), respectively [64,65,66]. Provided that ΔG_{HOM} for C-S-H precipitation remains fairly constant- a reasonable approximation, Eq. (18) suggests that C-S-H nucleation on quartz particles would be opposed by a greater energy barrier than on limestone if the specific free energy of bonding with C-S-H, $\gamma_{SL} - \gamma_{PS}$, is more positive for quartz than for limestone. This would be true if $\gamma_{SL,l} > \gamma_{SF,q}$ (i.e., the bare limestone-liquid interface has a greater average^{†††} specific energy than quartz) or also if $\gamma_{PS,l} < \gamma_{PS,q}$ (i.e., the C-S-H/limestone interface has a lower specific interface energy than the C-S-H/quartz interface). Datasets on solid-liquid interface energies for C₃S, calcite (the primary mineral component of limestone), and quartz are scant, subject to uncertainty [67,68], and are equally limited for interfaces involving C-S-H [69]. However, the limited datasets available do support our hypothesis that calcite (i.e., limestone) would provide a lower nucleation energy barrier for C-S-H nucleation than quartz. For example, measurements by Suzuki and Kasahara [68] suggest that the average quartz-water interface energy is very low, perhaps less than 10 mJ/m^2 but no greater than 100 mJ/m^2 , while calculations by Kvamme [67] indicate that the average calcite-water interface energy is in the range of $400\text{-}800 \text{ mJ/m}^2$. These values all would support the conclusions drawn from this study (see Eq. 18 and Figures 4, 5, 7, 9) that limestone provides more favorable sites for C-S-H nucleation than quartz ([41]). This kind of analysis has broad implications for quantifying the potential of various fillers to serve as “mineral acceleration agents”. In light of this

^{†††} We use the word ‘average’ to denote the fact that limestone is a polycrystalline rock comprising several minerals and that, in any case, even pure minerals such as quartz and calcite tend to have highly anisotropic surface energies.

analysis, the development of accurate and fully consistent information for benchmarking the interfacial interactions of mineral phases will be a key activity for advancing our ability to predict filler effects.

The third important factor that can influence reaction rates is the possible participation of dissolved species, liberated from the filler, in altering the course of hydration, either by precipitation of phases or by ion sorption reactions. Dissolved carbonate, in the presence of limestone has been shown to prevent the transformation of ettringite to monosulfate after gypsum is depleted because a carboaluminate phase is stabilized at the expense of monosulfoaluminate [70]. But this is likely a small effect, due to limited CO_3^{2-} -AFm formation at early ages [71]. The latter case (of ion exchange) is relevant, as the need for charge compensation which follows sorption of CO_3^{2-} ions on the C-S-H is expected to lead to the release of OH^- species which elevates the pH and hence the driving force for continuing/onward hydrate growth. This point provides insights on *compositional guidelines* which may be used to infer the impact of fillers on hydration. Based on the above discussion, it is clarified that limestone is a superior acceleration agent than quartz, even at equal AM values (i.e., surface area), because both its favored interfacial properties and its ability to induce CO_3^{2-} sorption can enhance the rates of both, nucleation and growth, respectively, of the cementitious hydration products at early ages.

6.0. Summary and Conclusions

This paper describes the generalized influence of mineral fillers on accelerating the rate of hydration reactions in cementitious materials. New simulation results are used to quantitatively interpret the role of dilution and the filler's characteristics on rates of reactions. Aspects of surface area, interfacial properties and ion exchange (i.e., sorption) reactions are distinguished and analyzed separately in terms of their influence on hydration rates. The results suggest that limestone is more effective than quartz (and certain other fillers) as an accelerant due to its interfacial properties and its ability to participate in ion exchange reactions. On a terminological and technological note, the community may begin thinking of limestone as

a *mineral additive* rather than a mineral filler because its ability to serve as a preferred surface and produce chemical (ion sorption) effects indicate its ability to serve as more than just a filler in cementing systems. Overall, the outcomes of this work shed new light on the *filler effect* and point the way to improved methods to better analyze, quantify, and screen minerals in terms of their ability to serve as cement replacement agents. Information of this nature is especially relevant in the context of enhancing prevailing cement replacement levels in concrete, the evaluation of new and superior filler agents and proportioning low-cement content concretes, such that, within limits, mechanical property development and concrete durability could remain largely unaffected, in spite of reductions in the cement content.

Acknowledgements

The authors gratefully acknowledge full financial support for this research provided by the University of California, Los Angeles (UCLA) and the National Science Foundation (CMMI: 1066583). The authors would also like to acknowledge the provision of materials by U.S. Concrete, OMYA A.G. and the U.S. Silica Company. The contents of this paper reflect the views of the authors, who are responsible for the accuracy of the datasets presented. This research was conducted in the Laboratory for the Chemistry of Construction Materials (LC²) and the core Molecular Instrumentation Center (MIC) at the University of California, Los Angeles (UCLA) and the Engineering Laboratory at the National Institute of Standards and Technology (NIST). The authors acknowledge the support of these laboratories in making this research possible. The last author would also like to acknowledge discretionary support provided by the Rice Endowed Chair in Materials Science.

References

¹ Concrete for the Environment. Published on Behalf of the Nordic Network Concrete for Environment by SP Swedish National Testing and Research Institute, Boras, Sweden, June 2003.

² Portland Cement Association Report, <http://www.cement.org/smreport09/>

-
- ³ V.T. Cost, Concrete sustainability versus constructability – closing the gap, International Concrete Sustainability Conference, Boston, 2011.
- ⁴ D.P. Bentz, E.F. Irassar, B. Bucher, W.J. Weiss, Limestone fillers to conserve cement in low w/c concretes: an analysis based on Powers' model, *Concrete International* 31 (2009) 41-46; and 31 (2009) 35-39.
- ⁵ V. Bonavetti, H. Donza, G. Menendez, O. Cabrera, E.F. Irassar, Limestone filler cement in low w/c concrete: a rational use of energy, *Cem. Concr. Res.* 33 (2003) 865–871.
- ⁶ D.P. Bentz, C.F. Ferraris, Rheology and setting of high volume fly ash mixtures, *Cem. Concr. Composites* 32 (2010) 265-270.
- ⁷ P.D. Tennis, M.D.A. Thomas, W.J. Weiss, State-of-the-art report on use of limestone in cements at levels of up to 15%, SN3148, Portland Cement Association, Skokie, Illinois, USA, 2011.
- ⁸ V.L. Bonavetti, V.F. Rahhal, E.F. Irassar, Studies on the carboaluminate formation in limestone filler-blended cements, *Cem. Concr. Res.* 31 (2001) 853-859.
- ⁹ W.A. Gutteridge, J.A. Dalziel, Filler cement: the effect of the secondary component on the hydration of Portland cement: Part 2: fine hydraulic binders, *Cem. Concr. Res.* 20 (1990) 853-861.
- ¹⁰ V. Rahhal, R. Talero, Early hydration of portland cement with crystalline mineral additions, *Cem. Concr. Res.* 35 (2005) 1285–1291.
- ¹¹ R.L. Sharma, S.P. Pandey, Influence of mineral additives on the hydration characteristics of ordinary Portland cement, *Cem. Concr. Res.* 29 (1999) 1525–1529.
- ¹² T. Sato, J.J. Beaudoin, Effect of nano-CaCO₃ on hydration of cement containing supplementary cementitious materials, *Adv. Cem. Res.* 23 (2010) 1-29.
- ¹³ D.P. Bentz, Modeling the influence of limestone filler on cement hydration using CEMHYD3D, *Cem. Concr. Composites* 28 (2006) 124-129.
- ¹⁴ N. Schwartz, N. Neithalath, Influence of a fine glass powder on cement hydration: comparison to fly ash and modeling the degree of hydration, *Cem. Concr. Res.* 38 (2008) 429–436.
- ¹⁵ J. Pera, S. Husson, B. Guilhot, Influence of finely ground limestone on cement hydration, *Cem. Concr. Composites* 21(1999) 99–105.
- ¹⁶ D.P. Bentz, Influence of water-to-cement ratio on hydration kinetics: simple models based on spatial considerations, *Cem. Concr. Res.* 36 (2006) 238-244.
- ¹⁷ S.S. Beedle, G.W. Groves, S.A. Rodger, Influence of fine pozzolanic and other particle on C₃S hydration, *Adv. Cem. Res.* 2 (1989) 3-8.

-
- ¹⁸ A. Kumar, et al, Simple methods to estimate the influence of limestone fillers on reaction and property evolution in cementitious materials, *Cem. Concr. Comp.* (submitted), 2012, pp. 16.
- ¹⁹ E.H. Kadri, S. Aggoun, G. De Schutter, and K. Ezziane, Combined effect of chemical nature and fineness of mineral powders on portland cement hydration, *Mater. Struct.* 43 (2009) 665-673.
- ²⁰ K. De Weerd, M. Ben Haha, G. Le Saout, K.O. Kjellsen, H. Justnes, B. Lothenbach, Hydration mechanisms of ternary portland cements containing limestone powder and fly ash, *Cem. Concr. Res.* 41 (2011) 279-291.
- ²¹ W.A. Gutteridge, J.A. Dalziel, Filler cement: the effect of the secondary component on the hydration of portland cement: Part 1: a fine non-hydraulic filler, *Cem. Concr. Res.* 20 (1990) 778–782.
- ²² A.R. Jayapalan, B.Y. Lee, S.M. Fredrich, K.E. Kurtis, Influence of additions of anatase TiO₂ nanoparticles on early-age properties of cement-based materials, *Trans. Res. Rec.* 2141 (2010) 41-46.
- ²³ J.J. Thomas, H.M. Jennings, J.J. Chen, Influence of nucleation seeding on the hydration mechanisms of tricalcium silicate and cement, *Journal of Physical Chemistry C*, 113(11), (2009), 4327-4334
- ²⁴ J.J. Thomas, A new approach to modeling the nucleation and growth kinetics of tricalcium silicate hydration, *J. Am. Ceram. Soc.* 90 (2007) 3282–3288.
- ²⁵ J.J. Thomas, J.J. Biernacki, J.W. Bullard, S. Bishnoi, J.S. Dolado, G.W. Scherer, A. Luttge, Modeling and simulation of cement hydration kinetics and microstructure development, *Cem. Concr. Res.* 41 (2011) 1257–1278.
- ²⁶ G.W. Scherer, J. Zhang, J.J. Thomas, Nucleation and growth models for hydration of cement, *Cem. Concr. Res.* doi:10.1016/j.cemconres.2012.03.019
- ²⁷ ASTM Standards Website: <http://www.astm.org/Standards/>
- ²⁸ A. Kumar, et al. Simple Methods to Estimate the Influence of Limestone Fillers on Reaction and Property Evolution in Cementitious Materials, submitted to *Cem. Concr. Comp.* (2012) pp. 10.
- ²⁹ T. Oey, A. Kumar, G. Sant, Unpublished Results, UCLA, 2012
- ³⁰ D.M. Kirby, J.J. Biernacki, The effect of water-to-cement ratio on the hydration kinetics of tricalcium silicate cements: Testing the two-step hydration hypothesis, *Cem. and Concr. Res.* (2012), pp. 10.
- ³¹ P. Sandberg, and L. Roberts, Cement-Admixture Interactions Related to Aluminate Control, *J. ASTM Inter.*, 2 (2005) 1-14.
- ³² R.J. Flatt, G.W. Scherer, J.W. Bullard, Why alite stops hydrating below 80% relative humidity, *Cem. and Concr. Res.* 41 (2011) 987-992.
- ³³ D.P. Bentz, M.A. Peltz, J. Winpigler, Early-age properties of cement-based materials: II influence of water-to-cement ratio, *ASCE J. Mater. Civil Eng.* 21(2009) 512-517.

-
- ³⁴ J. Zhang, E.A. Weissinger, S. Peethamparan, G. W. Scherer, Early hydration and setting of oil well cement, *Cement and Concrete Research*, 40, 1023—1033 (2010)
- ³⁵ V.K. Petersen and A.E. Whitten, Hydration processes in tricalcium silicate: application of the boundary nucleation model to quasielastic neutron scattering data, *Journal of Physical Chemistry C*, 113, 2347-2351 (2009)
- ³⁶ F. Ridi, E. Fratini, P. Luciani, P., F. Winnefeld, P. Baglioni, Tricalcium Silicate Hydration Reaction in the Presence of Comb-Shaped Superplasticizers: Boundary Nucleation and Growth Model Applied to Polymer- Modified Pastes, *Journal of Physical Chemistry C*, 116, 10887-10895 (2012)
- ³⁷ V.K. Peterson, M.C.G. Juenger, Hydration of tricalcium silicate: effects of CaCl₂ and sucrose on reaction kinetics and product formation, *Chem. Mater.* 18 (2006) 5798–5804.
- ³⁸ J.J. Thomas, A.J. Allen, H.M. Jennings, Hydration kinetics and microstructure development of normal and CaCl₂-accelerated tricalcium silicate (C₃S) pastes, *J. Phys. Chem. C* 113 (2009) 19836–19844.
- ³⁹ J.W. Cahn, The kinetics of grain boundary nucleated reactions, *Acta Metall.* 4 (1956) 449–459.
- ⁴⁰ J.J. Thomas, H.M. Jennings, “Effects of D₂O and mixing on the early hydration kinetics of tricalcium silicate,” *Chem. Mater.* 11 (1999) 1907–1914.
- ⁴¹ D. P. Bentz, T. Sato, I. De la Varga, and W. J. Weiss, Fine Limestone Additions to Regulate Setting in High Volume Fly Ash Mixtures, *Cement and Concrete Composites*, 34 (2012) 11-17.
- ⁴² T. Sato, and F. Diallo, Seeding effect of Nano-CaCO₃ on the hydration of tricalcium silicate, *Transportation Research Record*, 2141 (2010) 61-67.
- ⁴³ A. Kumar, Modeling the early-age hydration kinetics of cementitious systems, PhD Dissertation, Ecole Polytechnique Federale de Lausanne, Switzerland, 2012.
- ⁴⁴ A. Kumar, G. Sant, C. Patapy, C. Gianocca, K.L. Scrivener, The influence of sodium and potassium hydroxide on alite hydration: experiments and simulations, accepted by *Cem. Concr. Res.*, 2012.
- ⁴⁵ A. Kumar, S. Bishnoi, K.L. Scrivener, Modeling early age hydration kinetics of alite, *Cem. Concr. Res.* 42 (2012) 903-918.
- ⁴⁶ V. Kocaba, Development and evaluation of methods to follow microstructural development of cementitious systems including slags, PhD Dissertation, Ecole Polytechnique Federale de Lausanne, Switzerland, 2010.
- ⁴⁷ S. Bishnoi, K. L. Scrivener, Studying nucleation and growth kinetics of alite hydration using μ ic, *Cem. Concr. Res.* 39 (2009) 849-860.
- ⁴⁸ A. Quennoz, K.L. Scrivener, Hydration of C₃A–gypsum systems, *Cem. Concr. Res.* 42 (2012) 1032-1041.

-
- ⁴⁹ Given the large numbers of systems considered, due to space constraints, the fitting variables could not be included in the paper. However, if so desired, the reader is requested to contact the authors to source numerical values of the parameters used to fit the hydration rate curves, using both, the BNG and MRE formulations.
- ⁵⁰ T. Karapiperis, B. Blankleider, Cellular automaton model of reaction-transport processes, *Physica D* 78 (1994) 30-64.
- ⁵¹ J.W. Bullard, A three-dimensional microstructural model of reactions and transport in aqueous mineral systems, *Model. Simul. Mater. Sci. Eng.* 15 (2007) 711-738.
- ⁵² J.W. Bullard, A determination of hydration mechanisms for tricalcium silicate using a kinetic cellular automaton model, *J. Am. Ceram. Soc.* 91 (2008) 2088-2097.
- ⁵³ J.W. Bullard, R.J. Flatt, New insights into the effect of calcium hydroxide precipitation on the kinetics of tricalcium silicate hydration, *J. Am. Ceram. Soc.* 93 (2010) 1894-1903.
- ⁵⁴ D. Kaschiev, G.M. van Rosmalen, Review: nucleation in solutions revisited, *Cryst. Res. Technol.* 38 (2003) 555-574.
- ⁵⁵ R. Skapa, Optimum Sulfate Content of Portland Cement. PhD Dissertation, University of Aberdeen, pp. 320, 2009.
- ⁵⁶ L. Valentini, J.W. Bullard, G. Artioli, J-L. Traore, S.G. Satterfield, J.E. Terrill, M. Magistri, Role of sulfate incorporation in C-S-H during cement hydration: results from numerical modeling of the system C3S + gypsum, unpublished.
- ⁵⁷ L. Nachbaur, P.-C. Nkinamubanzi, A. Nonat, J.-C. Mutin, Electrokinetic properties which control the coagulation of silicate cement suspensions during early age hydration, *J. Colloid Interface Sci.* 202 (1998) 261-268.
- ⁵⁸ K.L. Scrivener, Modeling cement hydration: the end of the induction period to 28 days, Keynote Presentation at an International Workshop on Multiscale Modeling of Cementitious Materials, Krakow Institute of Technology, Poland, October 2012.
- ⁵⁹ P. Juilland, E. Gallucci, R.J. Flatt, K.L. Scrivener, Dissolution theory applied to the induction period in alite hydration, *Cem. Concr. Res.* 40 (2010) 831-844.
- ⁶⁰ Enthalpy data tabulated in the LLNL thermochemical database packaged with PHREEQC Version 2 Software. Available at http://wwwbrr.cr.usgs.gov/projects/GWC_coupled/phreeqc/
- ⁶¹ E.J. Garboczi, D.P. Bentz, Computer simulation of the diffusivity of cement-based materials, *J. Mater. Sci.* 27 (1992) 2083-2092.
- ⁶² A. Kumar, G. Sant, C. Patapy, C. Gianocca, K.L. Scrivener, The influence of sodium, potassium and calcium sulfates on alite hydration: experiments and simulations, submitted to *Cem. Concr. Res.*, 2012.

-
- ⁶³ G. Puerta Falla, The influence of CaCO₃ on cement hydration: Thermodynamics of reactions, Ph.D. Dissertation, University of California, Los Angeles, 2015 (in development).
- ⁶⁴ K. Sangwal, Additives and Crystallization Processes: From Fundamentals to Application, Wiley & Sons, New York, p. 468, 2007.
- ⁶⁵ I. Markov, Crystal Growth for Beginners: Fundamentals of Nucleation, Crystal Growth and Epitaxy, 2nd Edition, World Scientific, p. 566, 2004.
- ⁶⁶ S. Garrault, A. Nonat, Hydrated layer formation on tricalcium and dicalcium silicate surfaces: experimental study and numerical simulations, *Langmuir* 17 (2001) 8131–8138.
- ⁶⁷ B. Kvamme, T. Kuznetsova, D. Uppstad, Modeling excess surface energy in dry and wetted calcite systems, *J. Math. Chem.* 46 (2009) 756-762.
- ⁶⁸ T. Suzuki, H. Kasahara, Determination of the specific surface free energy of natural quartz crystals using measurement of contact angle of liquid droplets, *Cryst. Res. Technol.* 45 (2010) 1305-1308.
- ⁶⁹ S. Garrault-Gauffinet, A. Nonat, Experimental investigation of calcium silicate hydrate (C-S-H) nucleation, *J. Cryst. Growth* 200 (1999) 565-574.
- ⁷⁰ B. Lothenbach, G. Le Saout, E. Gallucci, K.L. Scrivener, Influence of limestone on the hydration of Portland cements, *Cem. Concr. Res.* 38 (2008) 848-860.
- ⁷¹ A. Ipavec, R. Gabrovsek, T. Vuk, V. Kaucic, J. Macek, A. Meden, Carboaluminate phases formation during the hydration of calcite-containing portland cement, *J. Am. Ceram. Soc.* 94 (2011) 1238,-1242.

Figure Captions

Figure 1: Particle size distributions for the: (a) cement, (b) limestone and (c) quartz used in this study. The uncertainty in the measured particle size distribution is around 6 %.

Figure 2: The correlation between the level (mass) of cement replacement and the change induced in the available solid surface area in the system for: (a) limestone and (b) quartz powders. The uncertainty in the calculated AM stems from the uncertainty inherent to the particle size analysis and is correspondingly around 6 %.

Figure 3: Measured heat evolution profiles for binary paste systems prepared for $w/s = 0.45$. For a given mixture, the uncertainty in the measured heat flow is around 2 % based on the heat flow measured on six replicate paste specimens between 1 hour and 72 hours.

Figure 4: (a and b) Measured heat profiles for plain and binary pastes for equivalent AM values and (c) measured heat profiles for plain cement pastes prepared at different w/c . For a given mixture, the uncertainty in the measured heat flow is around 2 % based on the heat flow measured on six replicate paste specimens between 1 hour and 72 hours.

Figure 5: The correlation between the area multiplier (AM) and parameters corresponding to the measured heat flow profiles: (a) slope of the acceleration regime and (b) heat rate at the main peak (c) inverse of time to main peak. In all graphs, the solid line fits the linear portion of the dataset and the dashed line projects a linear extrapolation. The thin solid lines show a 10 % bound to the best-fit line. For a given mixture, the uncertainty in the measured heat flow is around 2 % based on the heat flow measured on six replicate paste specimens between 1 hour and 72 hours.

Figure 6: Comparison of measured and BNG calculated heat profiles for paste mixtures. For a given mixture, the uncertainty in the measured heat flow is around 2% based on the heat flow measured on six replicate paste specimens between 1 hour and 72 hours.

Figure 7: (a) A comparison of the area factor (a_{factor}) plotted as a function of the area multiplier (AM) for systems simulated using the BNG mechanism and Product nuclei per gram of cement computed using the BNG approach as a function of: (b) replacement level for limestone systems (c) replacement level for quartz systems and (d) AM for limestone and quartz systems. Since the calculations are deterministic, for a given set of parameters the numerical solution shows no uncertainty.

Figure 8: A representative set of simulated and measured heat evolution profiles for paste systems. The complete datasets from experiments and simulations are provided in the supplementary information. For a given mixture, the uncertainty in the measured heat flow is around 2% based on the heat flow measured on six replicate paste specimens between 1 hour and 72 hours.

Figure 9: Product nuclei per gram of cement computed using the MRE approach as a function of: (a) replacement level for limestone systems, (b) replacement level for quartz systems and (c) AM for limestone and quartz systems. Since the calculations are deterministic, for a given set of parameters the numerical solution shows no uncertainty.

Figure 10: (a) Simulations of heat released during the hydration of a single C_3S particle ($5\ \mu\text{m}$ or $15\ \mu\text{m}$) with no limestone filler (Reference), 10 % replacement of limestone filler (10% Limestone) with lower energy barrier of C-S-H nucleation and 10% replacement of quartz filler (10% Quartz) with energy barrier of C-S-H nucleation identical to C_3S and (b) Simulated influence on hydration rates of carbonate anion sorption on the C-S-H. All curves represent a single simulation; multiple simulations on similar systems indicate that the reproducibility of any curve is within 2 % at any point.